LA-UR-05-4968

Title: | HYDRODYNAMIC MODELING OF DETONATIONS FOR STRUCTURAL DESIGN OF CONTAINMENT VESSELS

Author(s): | Edward A. Rodriguez
Christopher Romero

Los Alamos
NATIONAL LABORATORY
— EST.1943 —

HYDRODYNAMIC MODELING OF DETONATIONS FOR STRUCTURAL DESIGN OF CONTAINMENT VESSELS

Edward A. Rodriguez, PE
Engineering Sciences and Applications
Los Alamos National Laboratory
P.O. Box 1663, MS P946
Los Alamos, New Mexico 87544 USA
505-665-6195
erodriguez@lanl.gov

Christopher Romero
Dynamic Experimentation Division
Los Alamos National Laboratory
P.O. Box 1663, MS P940
Los Alamos New Mexico, 87544 USA
505-665-6250
cromero@lanl.gov

ABSTRACT

Los Alamos National Laboratory (LANL), under the auspices of the U.S. Department of Energy (DOE) and the National Nuclear Security Administration (NNSA), has been conducting confined high explosion experiments utilizing large, spherical, steel pressure vessels to contain the reaction products and hazardous materials from high-explosive (HE) events. Structural design of these spherical vessels was originally accomplished by maintaining that the vessel's kinetic energy, developed from the detonation impulse loading, be equilibrated by the elastic strain energy inherent in the vessel. In some cases, the vessel is designed for one-time use only, efficiently utilizing the significant plastic energy absorption capability of ductile vessel materials [1]. Alternatively, the vessel can be designed for multiple use, in which case the material response is restricted to the elastic range [2].

Within the last decade, designs have been accomplished utilizing sophisticated and advanced 3D computer codes that address both the detonation hydrodynamics and the vessel's highly nonlinear structural dynamic response. This paper describes the hydrodynamic modeling of HE reaction products phase, which produces transient pressures resulting in an impulsive load on the vessel shell. Modeling is accomplished through either (a) empirical/analytical methods utilizing a vast experimental database developed primarily for the Department of Defense (DoD) or (b) through application of numerical hydrodynamics codes, such as the Sandia National

Laboratories (SNL) shock-wave physics code, CTH [3], which accurately model the thermochemistry and thermophysics of a detonation. It should be noted that this paper only addresses blast load prediction using the methods stated and does not include an assessment of structural response methods.

1. INTRODUCTION

Containment vessels are used at Los Alamos to investigate the high-pressure shock-compression behavior of materials. This is accomplished through application of HE charges in driving materials, such as metals, into an extremely high-strain rate, high-pressure, and high-temperature regime. In many cases, the explosion products are hazardous, or the materials under compressions are radioactive. As such, care must be taken to contain and confine the explosion products and gases that trap hazardous and/or radioactive particulates.

Figure 1 depicts the LANL containment vessel, showing four ports on the horizontal axis for radiographic access. The top port is used for equipment entry and diagnostic cabling feed-through for monitoring the experiment. The experiment is situated inside a hexapod basket attached to the upper port nozzle flange. Figure 2 shows the Dual-Axis Containment System (DACS) comprised of a outer safety vessel, as a secondary barrier, and the inner containment vessel primary barrier. Each vessel is manufactured with forged nozzle assemblies to reinforce the radiographic entry and exit ports.
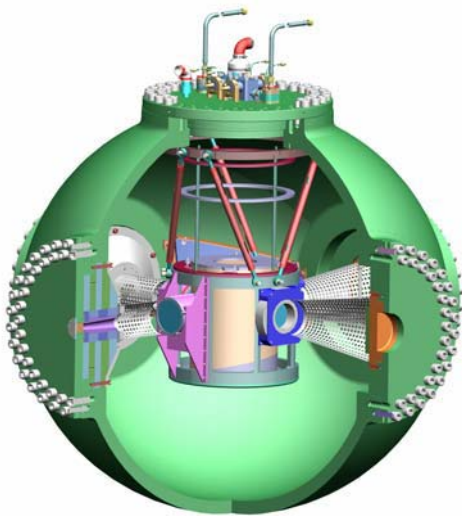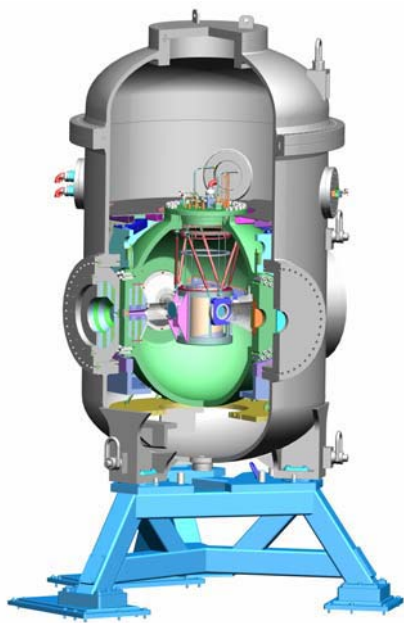
Figure 1. Dual-Axis Containment Vessel.

Figure 2. Dual-Axis Containment System (DACS)

The use of containment systems to mitigate explosion products is not only of concern to Los Alamos. The DoD laboratories, in collaboration with Sandia National Laboratories, have been designing and using these types of systems to destroy aged chemical and conventional weapon munitions [4]. Kobe Steel of Japan have designed and implemented similar destruction systems for aged chemical munitions [5], albeit on a much larger scale, that are being used not only in Japan but in the USA. These types of containment system would also be attractive to the

Department of Homeland Security for similar reasons. The major difficulty is that there are currently no industry standard design rules or guidelines for engineered containment vessels to withstand explosive detonations. More importantly to the ASME community, design rules for impulsively loaded containment vessels are not currently adopted in the ASME Code. Although Sec. III, Div. 1, attempted to discuss impulsive loadings in Appendix N, it has never been completed.

However, in 2002, ASME Code, Sec. VIII, Div. 3, Special Working Group on High-Pressure Vessels (SWG/HPV), formed the *Task Group (TG) on Impulsively Loaded Vessels* to help formulate rules and provide design guidance through a Code Case. Because structural response of a containment vessel is extremely complex, it becomes imperative to understand and quantify the explosion source term, or forcing function. Part of mandate for the TG on Impulsively Loaded Vessels of Sec. VIII, Div. 3, is to provide guidance on engineering solutions for explosive loading, and methods to determine the loading functions for subsequent structural analysis. The Sec. VIII TG has developed a Code Case, where much of the original work is detailed in Duffey, et al. [6,7], including description of empirical and analytical methods, as well as an elastic-plastic ductile failure design criteria, including fatigue crack-growth and fracture. However, this paper only addresses blast load prediction and does not include an assessment of computation dynamic response methods.

2. EMPIRICAL BLAST LOAD PREDICTION METHODS

Design manuals (e.g., TM 5-1300 [8] and DOE/TIC-11268 [9]) used for design of structures to resist the effects of accidental explosions have been based on principles of shock physics whereby the transient shock pressure is determined over the structure.

In explosions involving HE, blast waves from both single and multiple sources with bare or cased HE charges may exist. For this discussion, only single source HE explosions from bare, spherical, center initiated HE charges will be considered. References [8] and [9] contain details on multiple source explosions and cased HE charges. Figure 3 shows an ideal HE air blast wave structure. As the blast wave expands, it decays in strength, lengthens in duration, and slows down, both because of spherical divergence and because the chemical reaction is over,

except for afterburning, as the hot explosion products mix with the surrounding air [9].
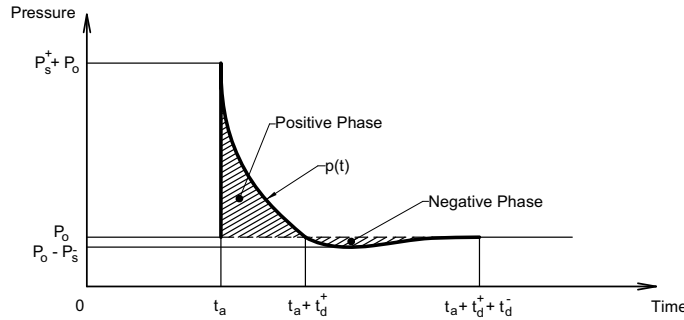

Figure 3. Ideal blast-wave structure

The blast parameters shown in Figure 3 are defined:

P_o = Ambient pressure

P_s^+ = Positive peak overpressure

P_s^- = Partial vacuum

t_a = Arrival time of blast wave to structure

t_d^+ = Duration of positive phase blast wave

t_d^- = Duration of negative phase blast wave

$p(t)$ = Pressure-time history of blast wave

The crosshatched areas in Figure 3 identify both the positive and negative impulses, I_s^+ and I_s^-. In most blast studies, the negative phase of the blast wave is ignored because $P_s^+ \gg P_s^-$ and $I_s^+ \gg I_s^-$ and only the blast parameters associated with the positive phase are considered.

TM 5-1300 shows that blast loads on structures can be divided into two main groups based on the confinement of the explosive charge (unconfined and confined explosions) and can be subdivided based on the blast loading produced. One of these blast loading parameters is referred to as a free-air burst whose explosion occurs in free air producing an initial output whose shock wave propagates away from the center of the detonation striking the protective structure without intermediate amplification of its wave. Free-air burst blast parameters from TM 5-1300 for a fully confined structure (internal gas) can be use for many blast-loaded containment vessel designs (e.g., spherical vessels and cylindrical vessels with a length-to-diameter ratio near one).

Full confinement of an explosion is associated with either total or near total containment of the explosion. Internal blast loads will therefore consist of unvented shock loads and very long duration gas pressures, which are a function of the degree of containment.

Blast curves in TM 5-1300 are plotted in terms of scaled distance from the HE charge to the structure,

$$Z = \frac{R}{W^{1/3}} \qquad (1)$$

where:

Z = Scaled Distance (ft/lb$^{1/3}$)
R = Distance to structure from center of HE (ft)
$W^{1/3}$ = Weight of TNT Equivalent HE (lb$^{1/3}$)

Pressure-time loadings from a HE detonation within a containment vessel can now be determined by utilizing the fundamental concepts of TNT-Equivalence, Blast Wave Structure, Blast Load Categories, and Scaled Distance.

It should be noted that the blast data provided in TM 5-1300 primarily relate to bare, spherical, center initiated HE detonations. Methods do exist, however, to account for different HE geometries and metal casings surrounding the explosive. Additionally, data are provided only for the first peak overpressure and associated impulse. Subsequent shock wave reflections (i.e., reverberations) from the inner surface of containment vessels after the initial detonation are often neglected because of their smaller scale relative to the initial pressure pulse. It should be noted, however, that subsequent shock wave reflections can be important in some systems, especially those designed with nonlinear response or where strong reflections occur on the order of the initial pulse. Hydrodynamic numerical simulations could be used to capture these shock wave reflections and details of the blast wave for more refined calculations.

Moreover, DOE/TIC-11268 presents a simplified method to account for these shock wave reflections using a 1.75 scaling factor for the initial peak overpressure and associated impulse. That is, for a centrally located detonation within a confined structure, it can be assumed that the second shock is half the amplitude and impulse of the initial reflected shock, the third shock is half the amplitude of the second reflected shock, and all later reflections are insignificant [9]. As previously inferred, the later two reflected pulses are often ignored in estimating the internal blast loading because the pressures and

impulses are much lower than the initial pulse. Because the combined loads from all three pulses are 1.75 times those from the initial pulse, a design simplification can be employed for structures with response times much longer than the longest time shown in Figure 4. This method simply combines all three pulses and multiplies the amplitude (and equally the impulse) by 1.75 [9] to achieve a single pulse of peak pressure and reflected impulse equal to 1.75 times the original values.
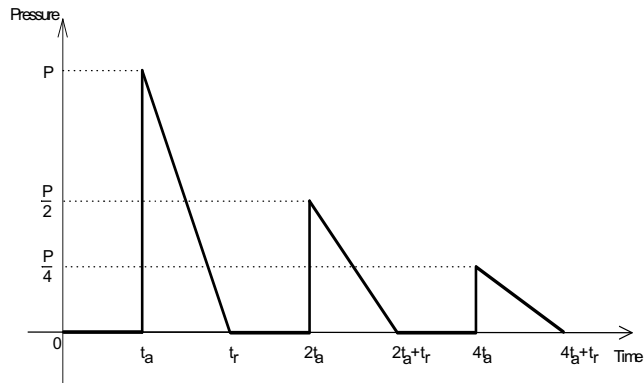

Figure 4.   Repeated Blast Loading Schematic in a Confined Structure [9].

Additionally, per DOE/TIC-11268, and as previously inferred, structural system response can be conservatively estimated by using only the first pulse when the natural period is less then one-tenth of t_r. Under these conditions, the structural response is sensitive to the suddenly applied peak pressure of the first pulse and rebound occurs slowly as the pressure reduces with time. The time phasing is such that the remaining pulses will result in smaller structural deflections.   Other structural response time conditions are also discussed in DOE/TIC-11268.

As indicated above, fully confined explosions, typical in blast containment vessel design, exhibit both an initial shock wave (i.e., impulse load) and a long-term quasi-static overpressure (residual, quasi-static pressure load).

TM 5-1300 provides methods for determining both these loading conditions using empirical data obtained from many DoD and DOE experiments. Figure 5 and Figure 6 are two sets of curves obtained from TM 5-1300 that can be used to determine pressure loadings in blast-loaded containment vessels.
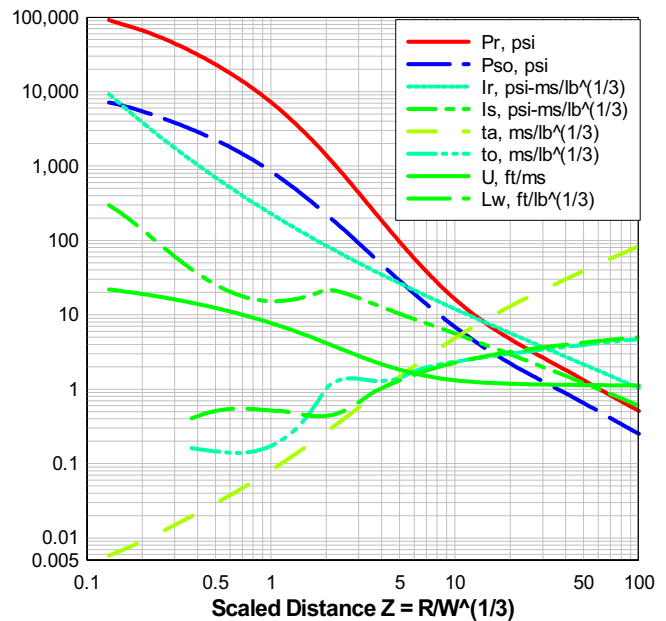

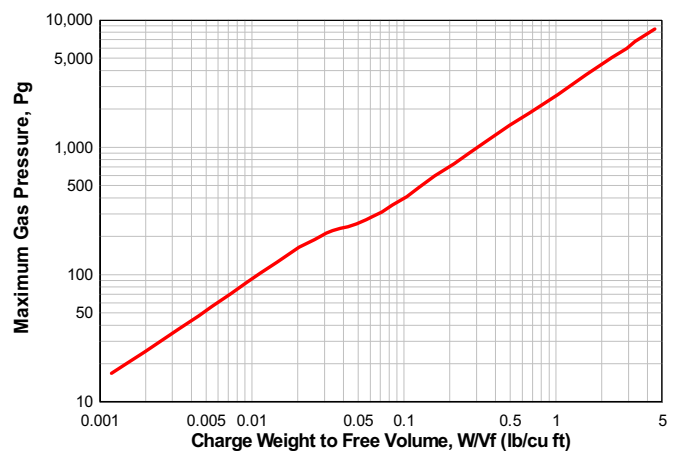Figure 5.   Positive phase shock wave parameters for a free-air burst [8].

Figure 6.   Peak gas pressure produced by a TNT detonation in a contained vessel [8].

The following information is used to obtain the blast parameters provided in TM 5-1300 or DOE/TIC-11268:

- HE Type
- HE Weight
- Distance from the HE Center to the Structure

Given this information, the following procedure for obtaining the blast data can then be applied:

- The HE weight is converted to a TNT-equivalent weight
- Per TM 5-1300 guidance, the TNT-equivalent weight is increased by 20% to compensate for accidental explosions or unknowns such as unexpected shock wave reflections, construction methods, quality of construction materials, etc.
- The scaled distance, Z, is determined knowing the distance to the structure and TNT-equivalent weight

Figure 5 is then used to obtain the following blast parameters knowing the value of the scaled distance, Z:

P_r = Peak positive normal-reflected pressure, psi

$\dfrac{I_r}{W^{1/3}}$ = Scaled unit positive normal reflected impulse, psi-ms/lb$^{1/3}$

$\dfrac{t_a}{W^{1/3}}$ = Scaled time of blast wave arrival, ms/lb$^{1/3}$

- The load duration, t_d is determined knowing I_r and P_r and by assuming a simple triangular pulse, or

$$t_d = \frac{2I_r}{P_r} \qquad (2)$$

- The internal free-volume, V_f, of the containment vessel is determined to obtain the residual quasi-static pressure
- The ratio of TNT-Equivalent Weight to Internal Free Volume is determined
- Residual pressure, P_{Residual}, is then obtained from Figure 6.

The pressure-time history is determined as shown in Figure 7.

Although empirical methods are highly used throughout the Department of Defense (DoD) community for design of structures, there are limitations to their use, as will be presented later in the comparison between empirical design and numerical hydrocode methods.
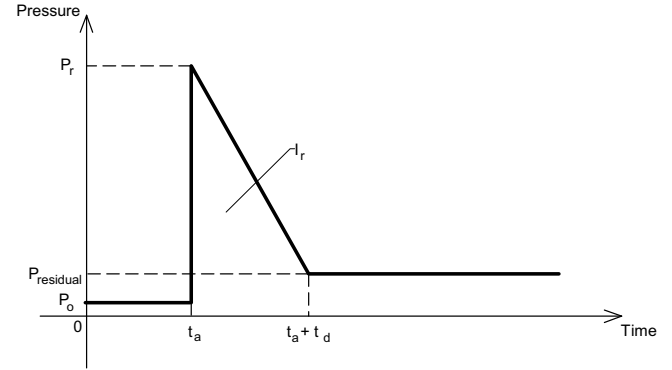

Figure 7. Pressure-time history using TM 5-1300 blast data [8].

3. HE DETONATION PHYSICS

HE detonation is a field of shock-wave physics that has been widely researched, with great advances occurring during the past half-century. The fundamental condition of a detonation is the creation of a shock-front that travels at speeds in excess of the sound speed. Shock waves form when disturbances in the fluid (or solid medium) propagate with a velocity greater than the sound speed. They are characterized by a steep front, and for metals, requires a state of uniaxial strain.

The particles (i.e., air for example) ahead of the shock-front are at ambient conditions (i.e., $P = P_o$, $\rho = \rho_o$, and $T = T_o$) while those immediately behind the shock-front are at shocked values (i.e., $P = P_1$, $\rho = \rho_1$, and $T = T_1$). Change in pressure, density, and temperature across the shock front is not gradual, nor along a gradient, but a discontinuous jump from unshocked to shocked values [10]. The shocked state is a step function from ambient conditions. The fundamental relations between the unshocked and shocked states are referred to as the "Jump" equations, yet more precisely known as the Rankine-Hugoniot equations [10-13]. These are developed from fundamental conservation equations: mass, momentum, and energy.

Mass

$$\frac{\rho_1}{\rho_0} = \frac{U_S - u_o}{U_S - u_1} \qquad (3)$$

5 Copyright © ASME 2005

If we assume that ahead of the shock front the particle velocity, $u_o = 0$, then:

$$\frac{\rho_1}{\rho_0} = \frac{U_S}{U_S - u_1} \tag{4}$$

or, immediately behind the shock front, there is an increase in density.

$$\rho_1 = \rho_o \left(\frac{U_S}{U_S - u_1} \right) \tag{5}$$

__Momentum__

$$P_1 - P_o = \rho_o (U_S - u_o)(u_1 - u_o) \tag{6}$$

Again, for conditions downstream where the particle velocity and pressure are assumed to be zero;

$$P_1 = \rho_o (U_S)(u_1) \tag{7}$$

__Energy__

$$E_1 - E_o = \frac{P_1 u_1 - P_o u_o}{\rho_o (U_S - u_o)} - \frac{1}{2}(u_1^2 - u_o^2) \tag{8}$$

Setting the initial downstream conditions to be zero for pressure and particle velocity;

$$E_1 - E_o = \frac{P_1 u_1}{\rho_o (U_S)} - \frac{1}{2}(u_1^2) \tag{9}$$

Substituting equation (5) for $\rho_o U_S$, yields the energy conservation in terms of pressure and particle velocity.

$$P u_1 = \frac{1}{2} \rho_o U_S u_1^2 + \rho_o U_S (E_1 - E_o) \tag{10}$$

where,

ρ = Density u = Particle velocity

P = Pressure U_S = Shock velocity

E = Specific internal energy

The subscripts (o, 1) in the above equations refer to the unshocked and shocked states respectively. There are five dependent variables and three equations, implying that an additional two relations are required to solve for shock wave characteristics.

The first required relationship is called an equation-of-state (EOS), which relates specific internal energy as a function of pressure and volume, $E = f(P,V)$. When combined with the jump energy equation, the specific internal energy term is eliminated, resulting in pressure as a function of volume relation $P = f(V)$, much like the Ideal Gas EOS relates gas expansion;

$$PV = nRT \tag{11}$$

However, it is not acceptable to use the Ideal Gas EOS for explosive reaction products, except in special instances. Detonation pressures and temperatures are of the order of several hundred thousand atmospheres and several thousand degrees Kelvin. A rule of thumb is that the ideal gas EOS, or the Nobel-Able modification to the ideal gas EOS, may be used when peak pressures are below 200 atmospheres and temperatures are less than 4000 degrees Kelvin. In most detonation examples, the pressures far-exceed 200 atm, and thus the ideal gas EOS is inappropriate.

The EOS is obtained through graphical or empirical representation of actual test data, which is commonly referred to as the "Hugoniot." The Hugoniot provides a relation between the shock velocity (U) and particle velocity (u_o), or through manipulation of the conservation equations, between shock pressure (P) and specific volume (v), i.e., reciprocal of density.
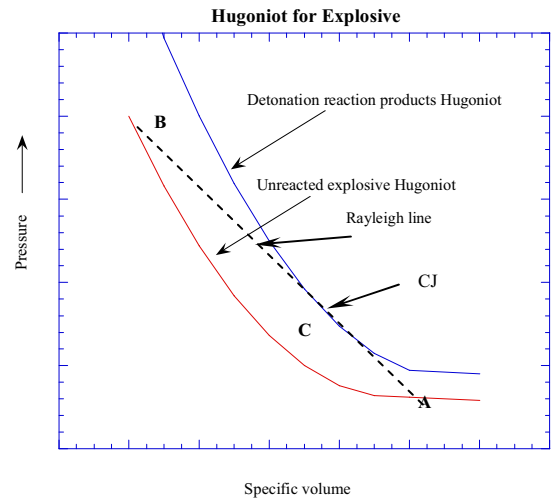

Figure 7. Hugoniot of unreacted and reacted HE.

The Hugoniot is a mathematical construct that results in all possible shock states of a material. A typical Hugoniot for an explosive is shown in Figure 7 for reacted and unreacted phases. The HE reaction "jumps" from point "A" to point "B" along the Rayleigh line. Where the Rayleigh line is tangent to the detonation products Hugoniot (Point "C"), this point is the CJ state, or the steady-state detonation.

For HE reaction products, the most widely accepted equation-of-state is the Jones-Wilkins-Lee (JWL) EOS [10-14], which was derived as an analytic fit to experimental data. It describes the pressure-volume-energy behavior of detonation reaction products in applications involving metal accelerations.

$$P = Ae^{-R_1 V/V_o} + Be^{-R_2 V/V_o} + C\left(\frac{V}{V_o}\right)^{-(1+\omega)} \quad (12)$$

where:

$A, B, C, R_1, R_2, \omega$ = JWL parameters (derived from experimental data)

V, V_o = Specific volumes; at pressure and initial states.

Successful use of the JWL EOS is highly dependent on problem type, where at extremely high compression densities, the results are suspect. The JWL EOS is primarily used with a "programmed burn" option, which specifies all the HE has reacted into gaseous products. That is, the reaction kinetics are completely ignored, assuming the HE is immediately converted to reaction products. A more suitable option is the history variable reactive burn (HVRB) for generalized problems, as this explicitly considers the reaction kinetics.

The final required relation to solve for the shock parameters is a specific value for one of the variables for a particular shock wave. A parameter well characterized by experimenters is the detonation velocity (D) of a particular explosive. The detonation velocity is related to the parameter termed the C-J (or Chapman-Jouguet) pressure. The C-J point is the state of the products immediately behind the detonation front. Knowing the HE detonation velocity, the "Jump" or Rankine-Hugoniot equations can now be written in terms of (D) instead of shock velocity (U).

$$\frac{\rho_{CJ}}{\rho_o} = \frac{D}{D - u_{CJ}} \quad (13)$$

or $$\rho_{CJ} = \rho_o\left(\frac{D}{D - u_{CJ}}\right) \quad (14)$$

The CJ pressure results from the above description and the Rankine-Hugoniot relations as;

$$P_{CJ} = \rho_o u_{CJ} D \quad (15)$$

where: D = detonation velocity, (mm/μs)

ρ_o = Unreacted HE density, (g/cm^3)

ρ_{CJ} = Reacted HE density, (g/cm^3)

u_{CJ} = Particle velocity at CJ state, (mm/μs)

4. NUMERICAL MODELING

Numerical modeling of hydrodynamic phenomena for the LANL containment system is accomplished with the Sandia National Laboratories (SNL) shock-wave physics code, CTH [3]. CTH is a family of codes developed at Sandia National Laboratories (SNL) for modeling complex multi-dimensional, multi-material problems that are characterized by large deformations and/or strong shocks. A two-step, second-order accurate Eulerian solution algorithm is used to solve the mass, momentum, and energy conservation equations. CTH includes models for material strength, fracture, porous materials, and HE detonation and initiation, as well as viscoplastic or rate-dependent models of material strength. The strength formulations of Johnson-Cook, Zerilli-Armstrong, and Steinberg-Guinan-Lund are standard options within CTH.

Hydrodynamic codes, as the name implies, are based on the fundamental equations of fluid mechanics; conservation of mass, momentum, and energy. The fluid medium is, of course, continuously deformable, has very little cohesion between particles, and may be compressible or incompressible [14]. For example, in the study of high-velocity penetration mechanics, the projectile and target interface is considered a fluid medium because impact stresses are of the order of 30-50 kbars (400,000 to 700,000 psi). Material strength at these high pressures is no longer significant. In other words, under these high pressures and velocities, the material "flows" much

7

Copyright © ASME 2005

like a fluid, hence hydrodynamic. Unlike Lagrangian meshes where the mesh/material distort, an Eulerian mesh is stationary in space, allowing material to move through each cell in the mesh.

The detonation of energetic material under shock loading conditions has been an area of great interest. As previously stated, recently developed model of reactive burn for HE has been added to CTH, which provides a more generalized solution for detonation problems. This model along with tabular EOS for the HE reaction products has been compared to 1D and 2D detonation experiments. Comparisons indicate excellent agreement of CTH predictions with experimental results. A reactive burn model (HVRB) coupled with advances in equation-of-state modeling make it possible to predict multi-dimensional burn phenomena without modifying model parameters for different dimensionality.

5. CONTAINMENT VESSEL MODEL

Herein the focus is on modeling the LANL 6-ft diameter HSLA-100 steel containment vessel to determine the impulsive load developed from detonation of a centrally detonated, bare spherical charge of PBX-9501. Figure 8 shows a schematic of the vessel and dimensions, with a spherical charge of PBX-9501 at the center of the vessel.
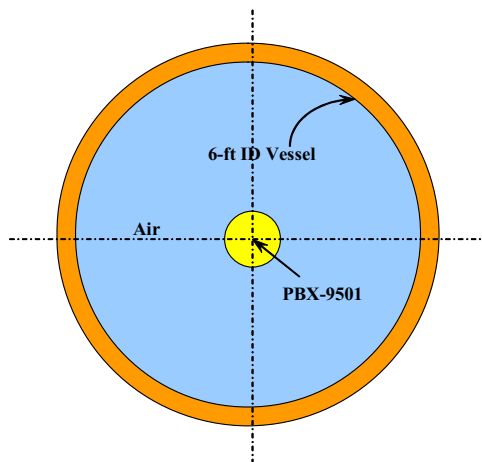

Figure 8. Vessel schematic

An Eulerian mesh encompassing approximately 400,000 cells, shown in Figure 9, represents the mathematical model tracking the pressure, temperature, density, and total energy of the system. Normal air makes up the bulk of the internal vessel

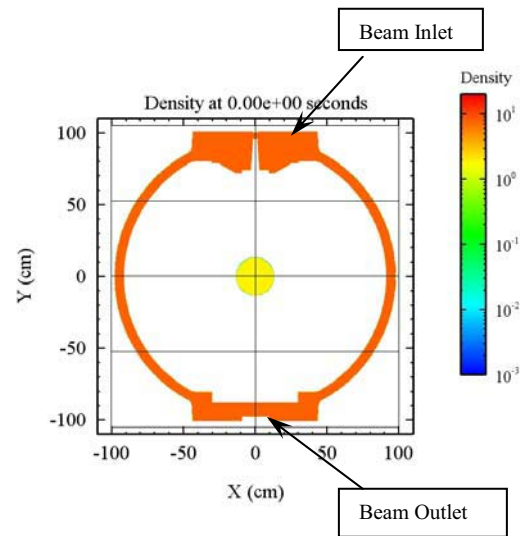volume, and the HSLA-100 vessel shell is modeled as 2.5-inch thick.

Figure 9. CTH 2D axisymmetric model.

Figure 9 also depicts details of the the entry and exit radiographic beam ports. These are especially crucial to model because of local pressure disturbances that arise during the transient event. The bare HE charge is centrally detonated within the sphere, in effect ensuring a purely spherical detonation wave throughout the HE.

Tracer particles (or stationary probes that track computed parameters), which monitor the pressure history of the incident and reflective blast wave, are embedded in the Eulerian mesh immediately inside the vessel shell, approximately 1.5 cell-widths away from the wall. A total of 43 tracer particles are modeled along the inner surface, including the radiographic entry and exit doors, which includes 13 tracer particles along the free-field spherical shell.

The JWL EOS is used for PBX-9501 [See Eq. 12] assuming adiabatic expansion (i.e., steady state expansion at constant entropy) with the following parameters [15]:

$$\rho_o = 1.84 \; g/cm^3$$
$$A = 8.524 \qquad R_1 = 4.55$$
$$B = 0.1802 \qquad R_2 = 1.30$$
$$C = 0.01207 \qquad \omega = 0.38$$

The CJ detonation velocity and pressure for PBX-9501 are:

$D_{CJ} = 8.805$ km/s $\qquad P_{CJ} = 34.47\,GPa$

Confined air is modeled using the SESAME EOS [3] for conditions at Los Alamos (7,500-ft above sea level) with the following parameters;

$\rho_o = 1.218E - 3\,g/cm^3$
$T_o = 298K \qquad c_o = 0.3388\,mm/\mu s$

where $\quad T_o =$ Reference temperature

$\qquad c_o =$ Sound speed

Material strength for the HSLA-100 steel shell is modeled using an elastic, perfectly-plastic model. A minimum hydrostatic tension failure pressure (or fracture pressure) is also included that provides the required pressure at which void nucleation is induced.

$S_y = 100\,ksi \qquad E = 30E6\,psi$

The steel shell also requires an equation-of-state for high-pressures, in this case a Mie-Grunesien EOS is employed. The equation relates the pressure in the solid continuum as a function of density (or inverse specific volume) and total energy, based upon a reference state of energy, pressure, and temperature E_H, P_H, T_H lying on the material Hugoniot.

The Gruneisen gamma formulation is based on statistical mechanics, equating energies of individual atoms to similar expressions in thermodynamics [16], and leads to a linear relationship between energy and pressure at constant density. The Gruneisen gamma, Γ, is assumed to be a function of density only, such that the pressure and energy terms result in;

$$P - P_H = \rho\Gamma\left(E - E_H\right) \qquad (16)$$

$$E - E_H = C_V\left(T - T_H\right) \qquad (17)$$

$$\Gamma = \rho^{-1}\left(\frac{\partial P}{\partial E}\right)_\rho \qquad (18)$$

and $C_V =$ Specific heat at constant volume.

The Hugoniot values for the Mie-Gruneisen EOS, P_H, E_H, T_H, are determined by employing the Rankine-Hugoniot "jump" equations with a linear, or quadratic, $U_S - U_P$ EOS model for the HSLA-100 steel material. The generalized $U_S - U_P$ model is

represented by Equation 19, where C_S is the bulk sound speed, and S_1 and S_2 are constants fitting the Hugoniot.

$$U_S = C_S + S_1 u_P + \left(\frac{S_2}{C_S}\right)u_P^2 \qquad (19)$$

For this problem, a linear $U_S - U_P$ provides accurate results for the shock and thermal response of the steel shell. Thermophysical properties used for HSLA-100 are:

$\rho_o = 7.85\;g/cm^3$
$C_S = 4.53\;km/s \qquad \Gamma = 1.84$
$S_1 = 1.50 \qquad\qquad S_2 = 0$

Figures 10 through 15 show the progression of the blast wave, from a 30-lb charge of PBX-9501, in terms of reaction products (i.e., gas) density contours. As can be seen from Figures 10 and 11, there is a density decrease at the interface of the unshocked air with the unreacted HE and reaction products. That is, the unreacted HE becomes a gaseous reaction and the density decreases to that slightly higher than air. Furthermore, there is a density increase at the shock front in accordance with to the conservation of mass equation.
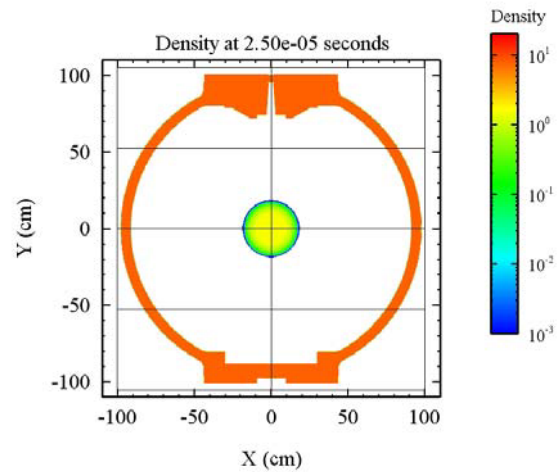

Figure 10. Detonation at 25 μs.

Figure 10 shows the HE charge 25μs after detonation, with much of the charge density still at 1.84 g/cm3, but towards the outer contour of the charge, it resembles gas densities. Figure 11 shows the blast wave at 125μs into the transient, with visible density difference radially outward towards the shell wall.
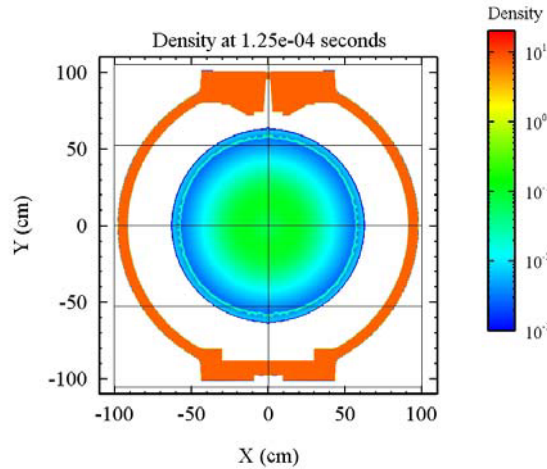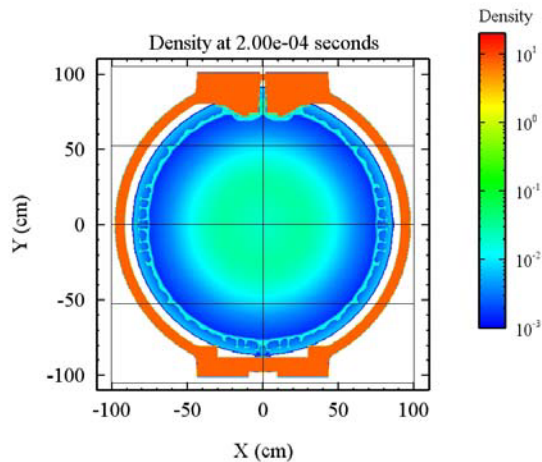
Figure 11. Detonation at 125 μs.

Figure 12. Detonation at 200 μs.

At about 200 μs, the incident blast wave reaches the vessel shell wall, as shown in Figure 12. At this point, the blast wave reflects back towards the center, as shown in Figure 13, thus continuing this process until a steady-state pressure has remained.

Although not altogether visible near the shell wall in Figure 13, slight physical instabilities occur. Among the best-known phenomena in fluid dynamics are the Rayleigh-Taylor and Kelvin-Helmholtz instabilities, which are found almost everywhere in nature. Rayleigh-Taylor instability occurs when a heavy fluid, superimposed on top of a lighter one in a gravitational field sinks into the lighter fluid. This results in the formation of spikes (sinking heavy fluids) and bubbles (rising light fluids).
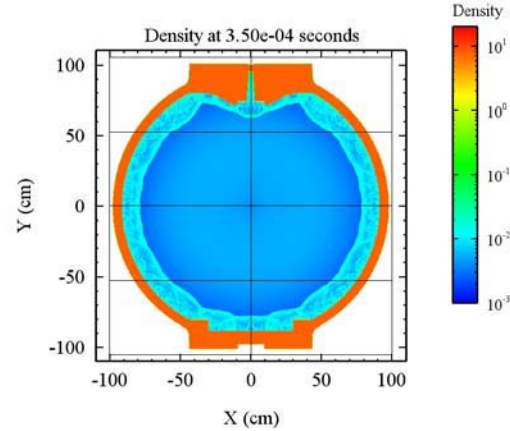

Figure 13. Detonation at 350 μs.

Another instability, commonly known as Kelvin-Helmholtz, occurs when two fluids of different density, separated by a plane surface, are in relative motion. This instability results in formation of eddies or vortices in the fluids. Notwithstanding the (real) physical Rayleigh-Taylor or Kelvin-Helmholtz instabilities, numerical instabilities also arise from model constraints, cell size, and mesh refinement.

As such, it is crucially important to distinguish between real phenomena and numerical problems. Figures 14 and 15 clearly depicts these physical Rayleigh-Taylor instabilities, creating local swirling of gases arising from the density differences.
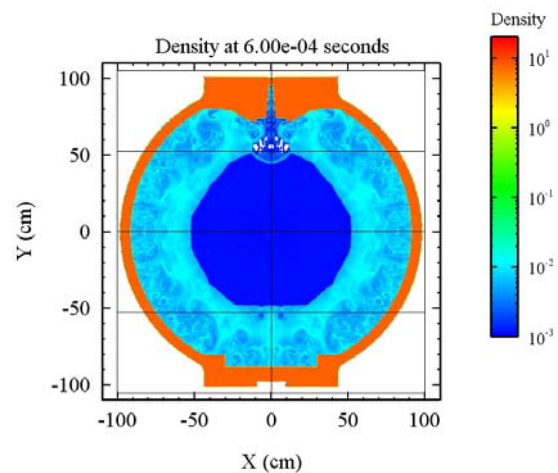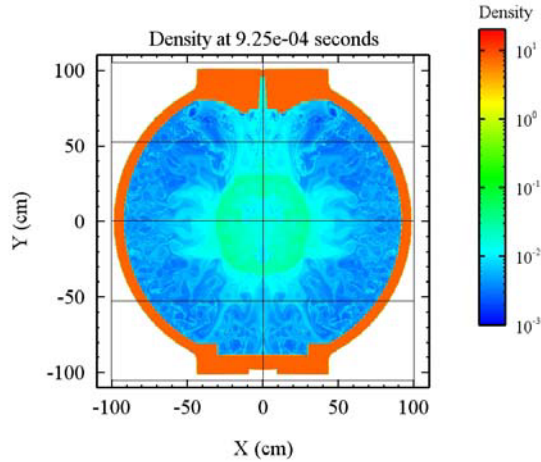

Figure 14. Detonation at 600 μs.

10

Figure 15. Detonation at 925 μs.

Figures 16 and 17 show the average pressure-time history from all tracer points within the free-field of the DACS shell for 30lb and 40lb bare spherical charge of PBX-9501. No tracer points in the vicinity of the radiographic beam inlet or outlet were used in averaging. Note, for visual clarity, the time scale on the P-T history plots of Figure 16 and Figure 17, have been moved upward by 1ms. As such, when the detonation blast wave first strikes the vessel wall at 200μs (see Figure 12), the actual time shown in Figure 16 and Figure 17 corresponds to 1200μs (or 1.2ms).
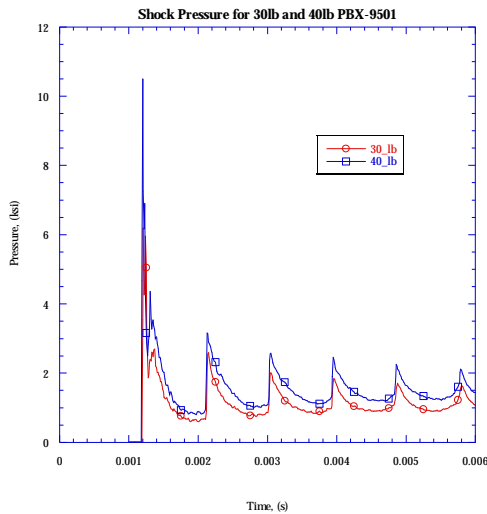

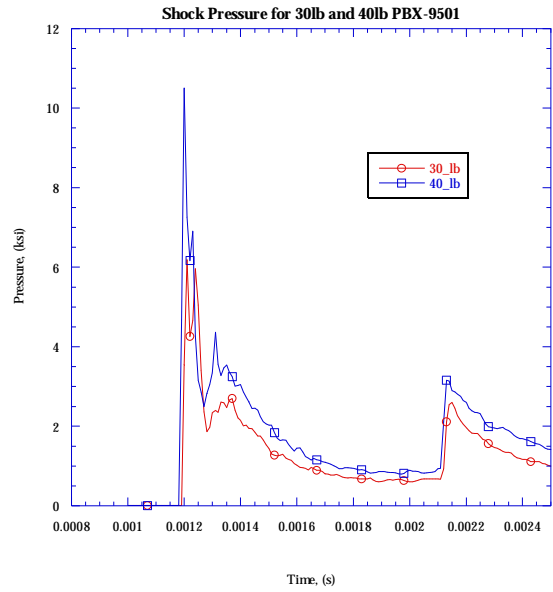Figure 16. P-T history for 30 and 40-lb. spherical charge of PBX-9501 in 6-ft ID vessel.

Figure 17. 30lb & 40lb P-T history – expanded time scale.

The total specific impulse in the system is merely the area under the P-T curve in Figure 16, excluding the pseudo-static pressure.

$$I_S = \int P dt \qquad (20)$$

It has been shown by Martineau [17] that the overall structural response of a system does not significantly increase by including all shock reflections (i.e., pressure reverberations) past the initial cycle. As such, the structural system is primarily driven by the "initial" specific impulse, or the area under the P-T curve to approximately 2ms in Figure 17. All subsequent pressure peaks (i.e., pressure reflections) are ignored for the structural analysis. As previously stated, additional pressure pulses from reflections can be important in some systems, especially those designed with nonlinear response or where strong reflections occur on the order of the initial pulse.

6. NON-SYMMETRIC LOADING

Certain loading conditions arise where the HE is not directly centered in the vessel system. These conditions pose a special design concern that, although the overall impulse is the same for a given charge, whether it is placed in the center or off-center, the structural response is totally different and might excite modes of vibration in the structure that

11

would not normally be observed. Furthermore, and more importantly, these special cases cannot easily be treated through empirical or analytical means because symmetry is not conserved. Therefore, testing and/or numerical hydrodynamics are the only recourse for quantitative solutions.
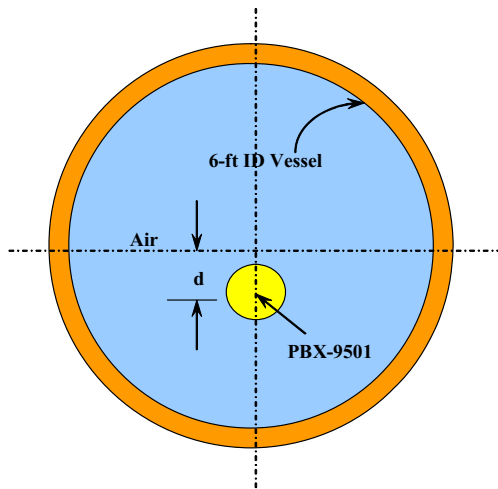

Figure 18. Off-center detonation for 40lb PBX-9501.

Figure 18 shows a bare spherical charge of PBX-9501 placed off-center by a distance, d, from the horizontal axis, just below the equatorial region. Figure 19 depicts the numerical model, showing dotted lines representing tracer particles near the vessel wall.   The actual vessel wall has been purposefully removed from Figure 19 to show the tracer particles. In this particular simulation, the HE sphere is placed half the distance from the horizontal centerline to the bottom of the vessel shell. At 100μs into the detonation event, the pressure wave is about to impinge on the south pole of the vessel shell. It must be appreciated that the P-T history for this event is non-uniform throughout the internal surface of the vessel, and each location of the inner vessel shell in the structural model must have a specified P-T history, which is different from the adjacent set.

Figure 20 shows the detonation event at 1000μs (i.e., 1ms). Here, the initial pressure pulse impinging at the top (north pole) of the vessel has been increased by a reflected pulse from the bottom. The discrete P-T history at each location on the vessel shell is different, thus increasing the complexity of the structural model as well.

Figures 21 and 22 show the pressure-time history for the south pole and north pole respectively. Because of HE proximity to the bottom of the vessel, i.e., half

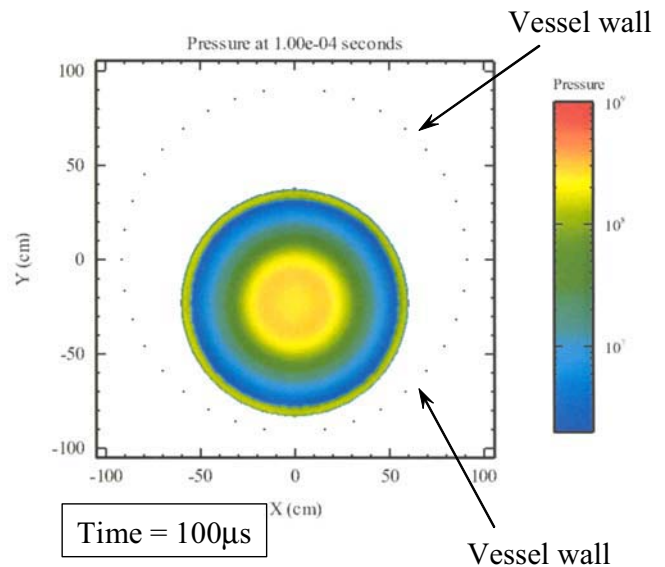the radius, the first pressure peak will be at the south pole, as shown in Figure 21, approximately at 0.20ms (20.0E-5 s).
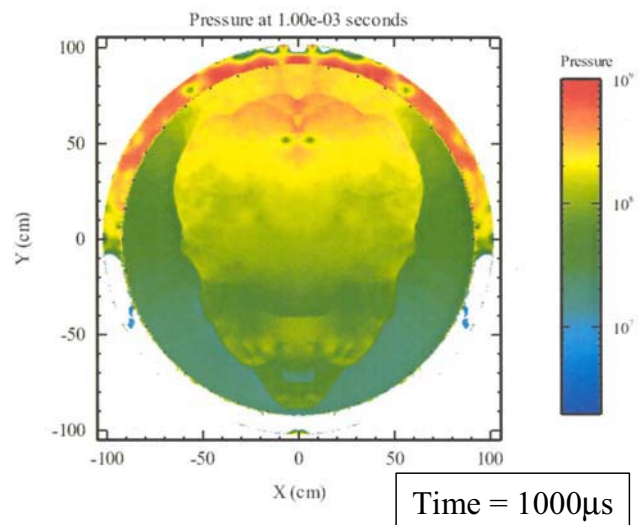

Figure 19. Off-center detonation for 40lb PBX-9501.

Figure 20. Off-center detonation for 40lb PBX-9501.

At approximately 0.40ms (40.0E-5 s) , the pressure reaches the north pole with slightly less magnitude, as shown in Figure 22.

However, this pressure peak is further reinforced immediately thereafter by the arrival of the reflected shock emanating from the bottom (i.e., south pole). This is shown by the second larger peak in pressure in Figure 22 at about 0.85ms (85.0E-5 s).

Likewise, shock reflections from the north pole arriving at the south pole are clearly shown at about 1.2ms to 2.0ms (120.0E-5 s to 200.0E-5 s) in Figure 21, while temporally in Figure 22 the pressure has reduced.
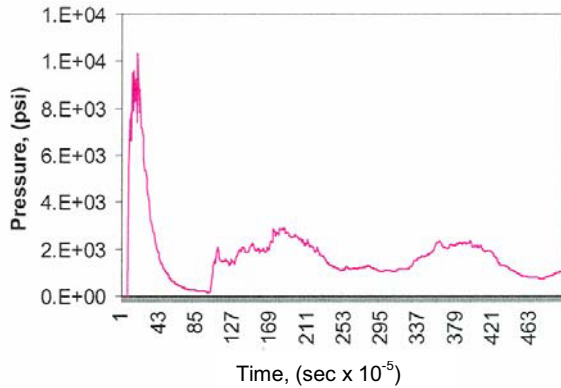

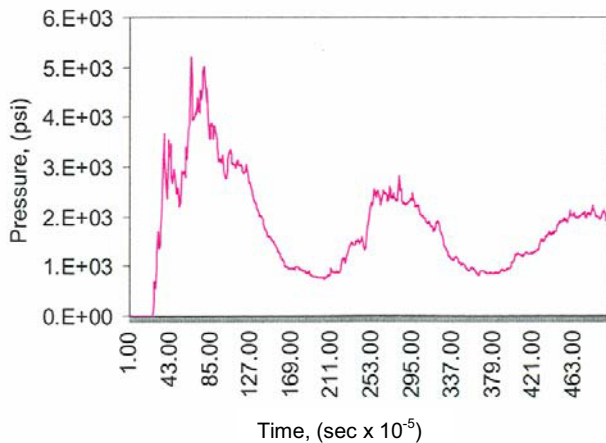Figure 21. South pole pressure pulse from off-center detonation.

Figure 22. North pole pressure pulse from off-center detonation.

Interestingly, at 0.85ms into the transient, the pressure at the south pole of the vessel has reduced in magnitude, which temporally corresponds to peak pressure at the north pole.

7. NUMERICAL AND ANALYTICAL COMPARISON

The empirical method described in Section 1 of this paper is used to determine the peak reflected pressure, P_R, and peak reflected impulse, i_R. A TNT-equivalence method is used herein for both HE compositions. Both, the Lawrence Livermore National Laboratory (LLNL) and TM5-1300 methods provide nearly identical results. Table 1 shows a comparison of both methods for a set of specified HE compositions. Theoretical density of TNT [$\rho = 1.654$ g/cm^3] is typically used with the LLNL method computations.

$$W_E = \frac{\Delta H_{Exp}^d}{\Delta H_{TNT}^d} W_{Exp} \qquad \text{TM5-1300 Method}$$

$$\eta = \frac{\left(\dfrac{\Delta H_{Exp}^d}{\rho_{o(Exp)}} \right)}{\left(\dfrac{\Delta H_{TNT}^d}{\rho_{o(TNT)}} \right)} \qquad \text{LLNL Method}$$

$$\eta = 0.2107 \left(\frac{\Delta H_{Exp}^d}{\rho_{o(Exp)}} \right)$$

Table 1
TNT Equivalence

HE	TNT Equivalence	
	TM5-1300	LLNL
TNT	1.00	1.00
HMX	1.26	1.27
PBX-9501	1.16	1.17
PBX-9502	0.84	0.85

Table 2 shows comparison of TM5-1300 and DOE/TIC-11268 to CTH numerical computations. Although results for TM5-1300 are in poor agreement, both in peak pressure determination and reflected impulse, the methodology used in DOE/TIC-11268 appear more reasonable, primarily due to addition of shock reflections after the initial first peak impulse. The results show that TM5-1300 computations under-predict the positive reflected impulse by as much as 47% for 30lb of PBX-9501 and 65% for 40lb of PBX-9502.

Table 2
Comparison CTH, TM 5-1300, DOE/TIC-11268

HE	W (lb)	CTH		TM 5-1300		DOE/TIC-11268	
		P_R (psi)	i_R (psi-ms)	P_R (psi)	i_R (psi-ms)	P_R (psi)	i_R (psi-ms)
PBX-9501	30	6190	1246	8465	848	14,814	1484
PBX-9502	40	6396	1358	8292	824	14,511	1442

Furthermore, TM 5-1300 computations <u>over-predict</u> the peak reflected pressure by 27% for PBX-9501 and 23% for PBX-9502. However, peak reflected pressure is inconsequential for providing the driving energy of a structure. Conversely, DOE/TIC-11268 provides a simplified method for reflected impulse computations by accounting for two subsequent shock reflections post initial pulse.

It should be generally noted that by using the scaling factor suggested by DOE/TIC-11268 (i.e., 1.75), which considers the reflected shocks, the reflected impulse is closer in line with the CTH results. Figure 23 shows a typical comparison of pressure-time history using the selected methods. Thus, in the absence of hydrodynamics codes that solve for detonation pressures, the simplified methods of DOE/TIC-11268 are recommended.
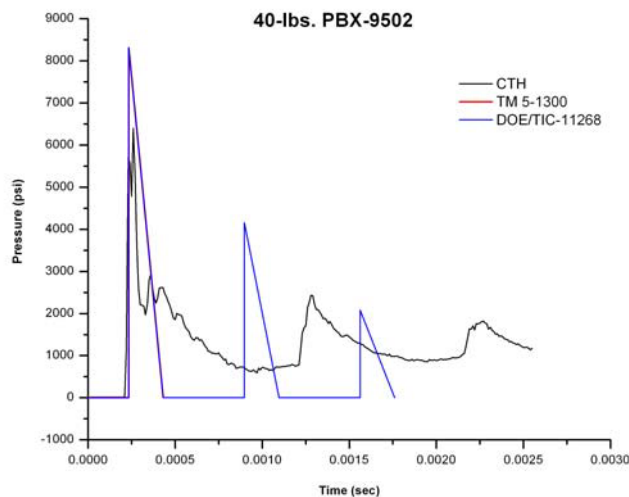

Figure 23. Comparison of numerical and analytical results for 40-lbs. PBX-9502.

8. RESULTS AND CONCLUSIONS

This paper has described engineering hydrodynamic methods for solution of detonation-induced pressure loading inside containment vessels. Empirical and analytical means based on TM5-1300 [8] and DOE/TIC-11268 [9] are intended for open air environments. However, the methods therein are appropriate for most engineering design problems that have some degree of structural symmetry and will require appropriate modification to yield suitable results for contained explosions in vessels. Although empirical methods, such as TM5-1300, appear to under-predict the peak reflected impulse as compared with hydrocodes, the guidelines specify increasing the actual HE mass (or weight) by 20% for design purposes to allow for uncertainties.

Thus, by including the 20% increase in HE mass to the previous TM5-1300 calculations, the reflected impulse, i_R, increases by 17%, yet the difference between CTH and TM5-1300 is 27% for PBX-9501 and ~40% for PBX-9502. Results comparison between empirical and numerical methods concludes that the TM5-1300 empirical methods under-predicts the overall reflected impulse, while DOE/TIC-11268 provides a nearly equal impulse response as CTH. Obviously, the implication of under-predicting the total specific impulse leads directly to a non-conservative structural response, and therefore a high-risk design.

Numerical hydrodynamic methods, such as the SNL code CTH, employ multi-physics and multi-material options allowing improved predictions of pressures, temperatures, and specific impulse. Hydrocode methods are especially useful and necessary when resolving non-symmetric detonations, resulting in non-uniform pressure-time histories, which must be detailed in the numerical structural model.

REFERENCES

[1] W. E. Baker, "The Elastic-Plastic Response of Thin Spherical Shells to Internal Blast Loading," *Journal of Applied Mechanics*, Vol. 27, pp. 139-144 (1960).

[2] J. J. White and B.D. Trott, "Scaling law for the Elastic Response of Spherical Explosion-Containment Vessels," *Experimental Mechanics*, Vol. 20, 174-177 (1980).

[3] E. S. Hertel, Jr, R. L. Bell, M. G. Elrick, A. V. Farnsworth, G. I. Kerley, J. M. McGlaun, S. V.

Petney, S. A. Silling, P. A. Taylor, and L. Yarrington, "CTH: A Software Family for Multi-Dimensional Shock Physics Analysis," in *Proceedings of the 19th International Symposium on Shock Waves*, held at Marseille, France, July 1993, pp. 377-382

[4] B. Haroldsen, M. Chiesa, J. Dike, Y. Kan, and R. Moehrle, "Explosive Destructive System: Fatigue Life Cycle Analysis," Sandia National Laboratories, August 15, 2000.

[5] J. Kiyoshi Asahina, "Detonation Chamber of Chemical Munitions: Its Design Philosophy and Operation," **2006 ASME Pressure Vessel and Piping Conference**, Vancouver, BC, CANADA, May 2006.

[6] T. A. Duffey, E. A. Rodriguez, C. Romero, "Design of Pressure Vessels for High Strain-rate Loading: Dynamic Pressure and Failure Criteria," **Welding Research Council**, Bulletin No. 477, December 2002.

[7] E. A. Rodriguez, and T. A. Duffey, Fracture-Safe and Fatigue Design Criteria for Detonation-Induced Pressure Loading in Containment Vessels," **Welding Research Council**, Bulletin No. 494, August 2004.

[8] Departments of the US Army, US Navy, and US Air Force, *Structures to Resist the Effects of Accidental Explosions*, Report AD-A243-272, US Army TM 5-1300, US Navy NAVFAC P-397, US Air Force AFR 88-22, November 1990.

[9] United States Department of Energy, *A Manual for the Prediction of Blast and Fragment Loadings on Structures*, DOE/TIC-11268, US Department of Energy, Albuquerque Operations Office, Amarillo Area Office, Pantex Plant, July 1992.

[10] P. W. Cooper, **Explosives Engineering**, VCH Publishers, New York, NY, 1996.

[11] J. A. Zukas and W. P. Walters, **Explosive Effects and Applications**, Springer Verlag, New York, NY, 1998.

[12] W. E. Baker, **Explosions in Air**, 2nd Edition, WE Baker Engineering, San Antonio, TX, 1983.

[13] W. Fickett and W. C. Davis, **Detonations; Theory and Experiment**, Dover Publications Inc., NY, 1979.

[14] M. L. Wilkins, **Computer Simulation of Dynamic Phenomena**, Springer-Verlag, New York, 1992.

[15] B. Dobratz, "LLNL Explosives Handbook: Properties of Chemical Explosives and Explosive Simulants," Lawrence Livermore National Laboratory, UCRL-52997, March 1981.

[16] M. A. Meyers, **Dynamic Behavior of Materials**, John Wiley and Sons, Inc., New York, NY, 1994.

[17] R. L. Martineau, "HSLA-100 Test Series Structural Analysis and Experimental Comparisons for Vessel Certification," Los Alamos National Laboratory document, Report No. DX-5:99-013, May 27, 1999.

ACKNOWLEDGMENTS